Int. J. Heat Mass Transfer. Vol. 35, No. 2, pp. 513–523, 1992
Printed in Great Britain

0017–9310/92 $5.00 + 0.00

High performance heat transfer ducts with parallel broken and V-shaped broken ribs

J. C. HAN and Y. M. ZHANG

Turbine Heat Transfer Laboratory, Department of Mechanical Engineering,
Texas A&M University, College Station, TX 77843, U.S.A.

(*Received* 7 *August* 1990 *and in final form* 8 *February* 1991)

Abstract—The effect of the broken rib orientation on the local heat transfer distributions and pressure drop in a square channel with two opposite in-line ribbed walls is investigated for Reynolds numbers from 15000 to 90000. The square channel is composed of ten isolated copper sections and has a length-to-hydraulic diameter ratio of 20. The rib height-to-hydraulic diameter ratio is 0.0625, and the rib pitch-to-height ratio equals 10. The results show that the 60° parallel broken rib or 60° V-shaped broken rib provides a higher heat transfer augmentation than the 45° parallel broken rib or 45° V-shaped broken rib and, subsequently, higher than the 90° broken rib. The parallel 'broken rib' or V-shaped 'broken rib' has 2.5–4 times heat transfer augmentation compared with the previous parallel 'continuous rib' or V-shaped 'continuous rib' with 2–3 times heat transfer augmentation for the same amount of 7–8 times pressure drop penalty.

INTRODUCTION

THIS STUDY investigates the effect of broken rib orientation on local heat transfer distributions and pressure drop in a square channel with two opposite ribbed walls for Reynolds numbers of 15000–90000. The square channel length-to-hydraulic diameter ratio (L/D) is 20; the rib height-to-hydraulic diameter ratio (e/D) is 0.0625; the rib pitch-to-height ratio (p/e) equals 10. Eight rib configurations are studied (see a–h in Table 1): 90° rib, 90° broken rib, 60° parallel broken rib, 60° V-shaped broken rib, 45° parallel broken rib, 45° V-shaped broken rib, 60° V-shaped broken rib A, 45° V-shaped broken rib A. The ribs on two opposite walls of the square channel are directly opposite each other (i.e. in-line arrays) for all eight configurations studied. The square channel has ten isolated copper sections in the axial direction. The regionally averaged heat transfer coefficients on both the ribbed-side and smooth-side walls of the channel are determined from the channel entrance to the downstream region. The channel averaged heat transfer coefficients are obtained, and the heat transfer vs pressure drop performances are compared for the eight rib configurations studied. The performances are also compared between the present 'broken' V-shaped and 'broken' parallel ribs and the previous 'continuous' V-shaped and 'continuous' parallel ribs. The semi-empirical friction and heat transfer correlations are also provided.

Casting turbulence promoters/ribs inside cooling passages is an effective technique to augment the heat transfer rate inside turbine blades. The ribs break the laminar sublayer of turbulent flow due to flow separation and reattachment in the opposite near wall region of the cooling channels. Therefore, the cooling effect is greatly improved. The effects of rib configurations (such as rib height, spacing, angle of attack) and flow Reynolds numbers on the average heat transfer and pressure drop in the fully developed region of a uniformly heated square channel with two opposite rib-roughened walls were investigated systematically [1, 2]. The effects of the above parameters on the local heat transfer and pressure drop in developing (entrance) and fully developed regions of foil-heated, ribbed rectangular channels with five different aspect ratios were reported [3–5]. The results show that the parallel angled ribs (the ribs on two opposite walls of the cooling channels are in parallel orientation) provide a better heat transfer performance than the transverse ribs, and the narrow aspect ratio channels (near the leading edge of the airfoil) perform better than the broad aspect ratio channels (near the trailing edge of the airfoil). The angled ribs provide a better heat transfer performance

Table 1. Configurations of ribs on channel walls

Case	Description in text	Notation in figures
a	90° continuous rib	90° ||
b	90° broken rib	90° ||
c	60° parallel broken rib	60° //
d	45° parallel broken rib	45° //
e	60° V-shaped broken rib	60° \/
f	45° V-shaped broken rib	45° \/
g	60° V-shaped broken rib A	60° \/
h	45° V-shaped broken rib A	45° \/
i†	60° parallel continuous rib	60° //
j†	45° parallel continuous rib	45° //
k†	60° V-shaped continuous rib	60° \/
l†	45° V-shaped continuous rib	45° \/

† Results reported in ref. [11].

NOMENCLATURE

A	heat transfer surface area
D	square channel width or height
e	rib height
e^+	roughness Reynolds number
f	friction factor in a channel with two opposite ribbed walls
f_o	friction factor in fully developed tube flow
f_r	friction factor for four-sided ribbed channel
G	heat transfer roughness function; also mass velocity, ρV
$\bar{G}$	average heat transfer roughness function
g_c	conversion factor
h	heat transfer coefficient
K	thermal conductivity of air
L	channel length
Nu	Nusselt number, hD/K
Nu_o	Nusselt number in fully developed tube flow
Nu_r	ribbed-side wall Nusselt number
Nu_s	smooth-side wall Nusselt number
P	rib pitch
Pr	Prandtl number of air
ΔP	pressure drop across the test section
q	heat generation rate from foils
q_{loss}	heat loss rate through insulation
R	momentum transfer roughness function
Re	Reynolds number, $(\rho DV)/\mu$
St	Stanton number, $Nu/(Re\ Pr)$
St_o	Stanton number in fully developed tube flow
St_r	ribbed-side wall Stanton number
St_s	smooth-side wall Stanton number
T_b	bulk mean temperature
T_w	local wall temperature
V	average velocity of air
X	axial distance from heated channel inlet.

Greek symbols

μ	average dynamic viscosity of air
ρ	average density of air.

than the transverse rib because of the secondary flow induced by the rib angle in addition to breaking the laminar sublayer in the opposite near wall region. The rib angle effect diminishes in the broad aspect ratio channels because the ribs on two opposite walls are too close to each other. The rib angle induced secondary flow is reduced. In a two-pass square channel, in addition to the rib turbulators and the flow Reynolds number, the effects of the sharp 180° turn on the distributions of the local mass transfer (using the naphthalene sublimation technique) and pressure drop right after the sharp turn are significant [6–8]. Effects of the rib-angle orientations on the local mass transfer (using the naphthalene sublimation technique) and pressure drop distributions in three-pass rectangular channels have also been reported [9, 10]. These previous studies show that rib angle orientations on two opposite walls of a cooling channel have a significant impact on the local heat transfer and pressure drop distributions.

Reference [11] recently re-examined the effect of the rib angle orientation on the local, regionally averaged heat transfer distributions and pressure drop in a square channel with two opposite in-line ribbed walls (see i–l in Table 1). The results show that the continuous V-shaped rib does better than the continuous parallel rib and, subsequently, better than the continuous crossed rib (the ribs on two opposite walls of the cooling channels are in crossed orientation) and the transverse rib. The V-shaped continuous rib produces the highest heat transfer augmentation while the continuous crossed rib has the lowest heat transfer enhancement and the smallest pressure drop penalty. This is because the V-shaped continuous rib induces a four-cell secondary flow while the parallel continuous rib has two-cell secondary flow, but the crossed continuous rib only produces a one-cell secondary flow in addition to breaking the laminar sublayer in the opposite near wall region of the cooling channels.

The above studies consistently indicate that high heat transfer augmentation can be achieved by increasing the number of rib angle induced secondary flow cells in the opposite near wall region of the cooling channels. It is of interest whether the 'broken' V-shaped or 'broken' parallel ribs can perform even better than the 'continuous' V-shaped or 'continuous' parallel ribs that are reported in ref. [11]. The reason is that the broken V-shaped or broken parallel ribs may create more secondary flow cells and produce more local turbulence in the opposite near wall region than the continuous V-shaped or continuous parallel ribs. To obtain the true average heat transfer coefficients for turbine cooling design, it is better to have a test section that can determine the regionally averaged heat transfer coefficients in the channel streamwise flow direction. The regionally averaged heat transfer method has been previously used [11–13]. The same technique is employed for this study.

Considerable data are available for rib-roughened heat transfer and pressure drop in the flow passages of different cross-sectional areas. For example, fully developed turbulent flow heat transfer and friction were reported for flow in ribbed circular tubes [14–16], between ribbed parallel plates [17], in ribbed triangular ducts [18], and in ribbed annular ducts [19,

20]. This study focuses on the augmented heat transfer in ribbed square ducts.

EXPERIMENTAL APPARATUS AND DATA REDUCTION

Experimental apparatus

The test duct is divided into ten short copper sections as seen in Fig. 1(a). Each copper section is composed of four copper plates 10.16 cm (4 in.) long, 0.63 cm (0.25 in.) thick and has an inner cross-section of 5.08 cm by 5.08 cm (2 in. by 2 in.). Thin wood strips (0.159 cm thick) are adhered along the periphery contact surface between copper sections as insulation to prevent possible heat conduction. The square test duct has a length-to-hydraulic diameter ratio (L/D) of 20. The local wall temperature of the test duct is measured by 80 copper–constantan thermocouples distributed along the length and across the span of the copper plates. There is an unheated entrance duct (not shown in Fig. 1(a)) that has the same cross-section and length as that of the test duct, although the entrance duct is of Plexiglas plates. This entrance duct serves to establish hydrodynamically fully developed flow at the entrance to the test duct. Figure 1(b) shows a schematic of the rib geometry. The ribbed wall was made by gluing copper ribs of square cross-section to the copper plates in a required distribution and orientation. The glue thickness is uniform and less than 0.0127 cm. The rib height-to-hydraulic diameter ratio (e/D) is 0.063, the rib pitch-to-height ratio (P/e) equals 10 for the eight rib configurations studied.

Figure 1(c) shows the cross-section of the test duct. The test duct has an inner cross-section of 5.08 cm by 5.08 cm. The test duct orientation is such that the two opposite ribbed walls of the square cross-sections are vertical and the two opposite smooth walls horizontal. The foil heaters are uniformly cemented between the

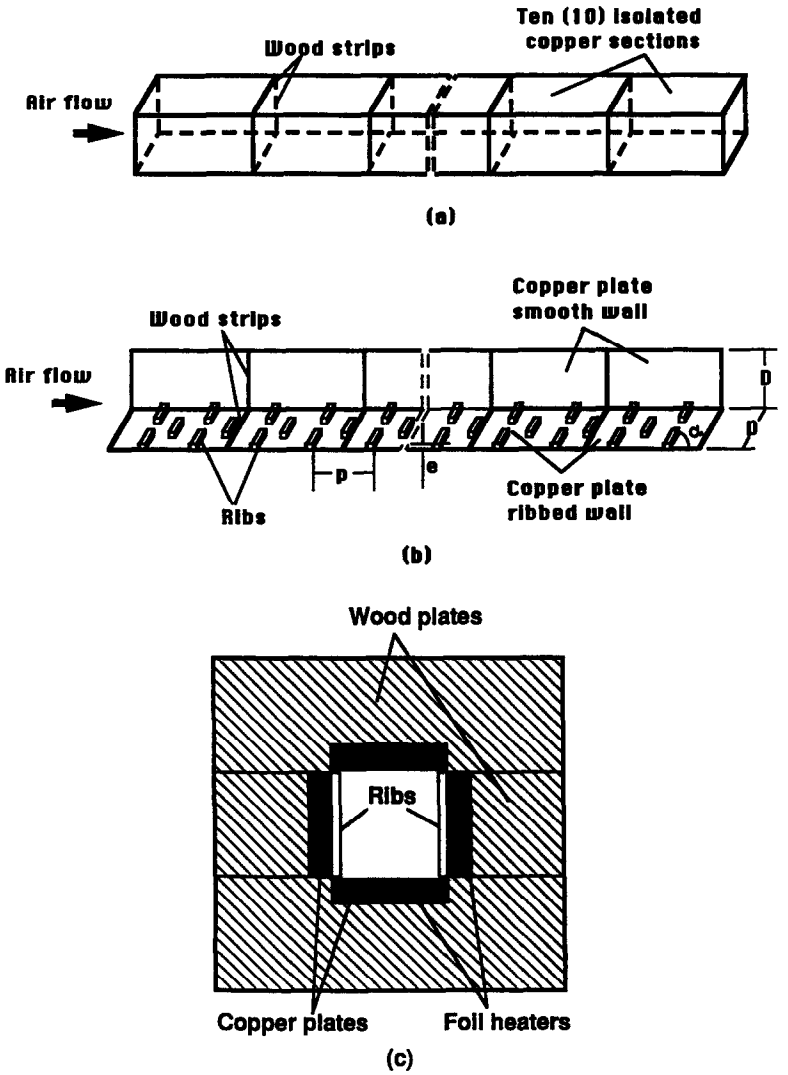

FIG. 1. (a) Test duct composed of ten copper sections; (b) rib orientation; (c) cross-section of the test duct.

copper plate backface and a wood plate to insure good contact. Each of the four duct walls has one foil heater with each heater independently controlled by a variac transformer. Each heater provides a controllable uniform heat flux for each duct wall. The smooth side walls are isolated from the ribbed side walls to eliminate heat conduction (see Fig. 1(c)). The entire heated test duct is insulated by fiberglass material.

Thermocouples are also used to measure the bulk mean air temperature entering and leaving the test duct. A 100-channel data logger and a computer are used for temperature readings and data storage. Two pressure taps at the inlet and outlet of the test duct are used for the static pressure drop measurements.

Data reduction

A micro-manometer connected to pressure taps measures the pressure drop across the test duct. In fully developed duct flow, the friction factor was determined by measuring the pressure drop across the test duct and the mass velocity of air as

$$f = \Delta P/[4(L/D)(G^2/2\rho g_c)]. \quad (1)$$

The friction factor is based on the isothermal conditions (tests without heating). The maximum uncertainty in the friction factor (primarily due to the pressure drop and mass flow rate measurements) was estimated to be less than 8% for Reynolds numbers greater than 10000 by using the uncertainty estimation method of Kline and McClintock [21]. To reduce the effect of Reynolds number on the friction factor increment, the friction factor of the present study was normalized by the friction factor for fully developed turbulent flow in smooth circular tubes ($10^4 < Re < 10^6$) proposed by Blasius [22] as

$$f/f_o = f/[0.046Re^{-0.2}]. \quad (2)$$

The local heat transfer coefficient was calculated from the local net heat transfer rate per unit surface area to the cooling air, the local wall temperature on each copper plate, and the local bulk mean air temperature as

$$h = (q - q_{loss})/[A(T_w - T_b)]. \quad (3)$$

This equation was used for the ribbed side wall and smooth side wall heat transfer coefficient calculations. The local net heat transfer rate was the electrical power generated from the foil heaters minus the heat loss outside the test duct. The electrical power generated from the foil was determined from the measured foil resistance and voltage for each wall of the test duct. The effect of the local wall temperature variation on the local foil resistance was estimated to be very small and negligible. To place the results on a common basis, the heat transfer area used in equation (3) was always that of a smooth wall. The foil provided a nearly uniform heat flux on each wall of the test duct. The heat loss from the test duct was determined experimentally under a no flow condition. The maximum heat loss from the ribbed side wall and smooth side wall was estimated to be less than 3 and 4%, respectively, for Reynolds numbers greater than 10000.

The local wall temperatures used in equation (3) were read from the thermocouple output of each copper plate. The local wall temperatures on both the ribbed and smooth side walls were close to each other within 1°C. The bulk mean air temperatures entering and leaving the test duct were measured by thermocouples. The local bulk mean air temperature used in equation (3) was calculated from the measured inlet air temperature and the net heat input to the air. The total net heat transfer rate from the test duct to the cooling air agreed with the cooling air enthalpy rise along the test duct. The inlet bulk mean air temperature was 27–31°C (81–88°F) depending on the test conditions. The maximum uncertainty in the Nusselt number (primarily due to the heat transfer rate and the wall temperature measurements) was estimated to be less than 8% for Reynolds numbers larger than 10000 by using the uncertainty estimation method of Kline and McClintock [21].

To reduce the effect of Reynolds number on the heat transfer augmentation, the local Nusselt number of the present study was normalized by the Nusselt number for fully developed turbulent flow in smooth circular tubes correlated by McAdams [22] as

$$Nu/Nu_o = (hD/K)/[0.023Re^{0.8}\,Pr^{0.4}]. \quad (4)$$

Friction and heat transfer correlations. The friction data for turbulent flow in a square duct with two opposite ribbed walls can be correlated by the following equations [3]:

$$R(e^+) = (f_r/2)^{-1/2} + 2.5\ln(2e/D) + 2.5 \quad (5)$$

where

$$f_r = 2f - f_o \quad (6)$$

$$e^+ = (e/D)Re(f_r/2)^{1/2}. \quad (7)$$

The heat transfer data for fully developed turbulent flow in a square duct with two opposite ribbed walls can be similarly correlated by the following equations [3]:

$$G(e^+) = [(f_r/2)^{1/2}]/St_r + 2.5\ln(2e/D) + 2.5 \quad (8)$$

and

$$\bar{G}(e^+) = [(f_r/2)^{1/2}]/\overline{St} + 2.5\ln(2e/D) + 2.5 \quad (9)$$

where

$$\overline{St} = (St_r + St_s)/2. \quad (10)$$

In the present data reduction program, equations (5)–(10) were used to calculate the friction roughness function $R(e^+)$ and the heat transfer roughness function $G(e^+)$ and $\bar{G}(e^+)$.

EXPERIMENTAL RESULTS AND DISCUSSION

Regionally averaged heat transfer data

Figure 2 shows the top view of the studied eight rib orientations: 90° continuous rib, 90° broken rib, 60° parallel broken rib, 45° parallel broken rib, 60° V-shaped broken rib, 45° V-shaped broken rib, 60° V-shaped broken rib A, and 45° V-shaped broken rib A. Four rib orientations reported in ref. [11] are also included for comparison: 60° parallel continuous rib, 45° parallel continuous rib, 60° V-shaped continuous rib, and 45° V-shaped continuous rib. Table 1 lists the rib orientation and its corresponding notation shown in the following figures.

The local (regionally averaged) heat transfer results are presented as the axial distributions of a normalized Nusselt number ratio. Figure 3 shows the Nusselt number ratio distributions for the four-side smooth channel. The Nusselt number ratio decreases with increasing axial distance and then reaches a constant value in the fully developed region at a given flow Reynolds number. The local Nusselt number ratio decreases slightly with increasing Reynolds numbers. For the four-side smooth channel the maximum deviation of the Nusselt number from the McAdams [22] correlation is 10%.

Figures 3–6 present the test results for the ribbed channel. These figures represent the ribbed-side Nusselt number ratio distributions and the corresponding smooth-side Nusselt number ratio distributions for broken 90°, 60° and 45° parallel and V-shaped ribs. It was found from the experimental raw data that the local temperatures on two opposite walls are about the same at the same axial distance from the inlet of the heated channel. Therefore, the local ribbed-side Nusselt number in these figures is the average value of the two opposite ribbed-wall Nusselt numbers at a given location, and the local smooth-side Nusselt

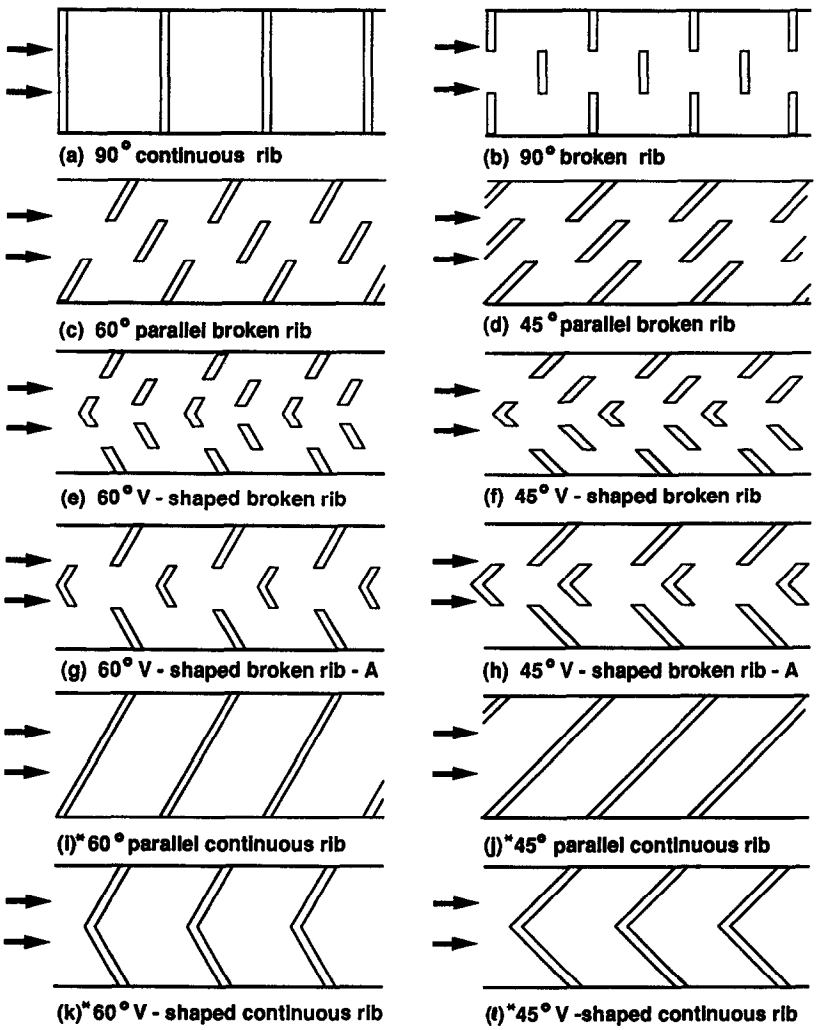

FIG. 2. Top view of studied rib orientations.

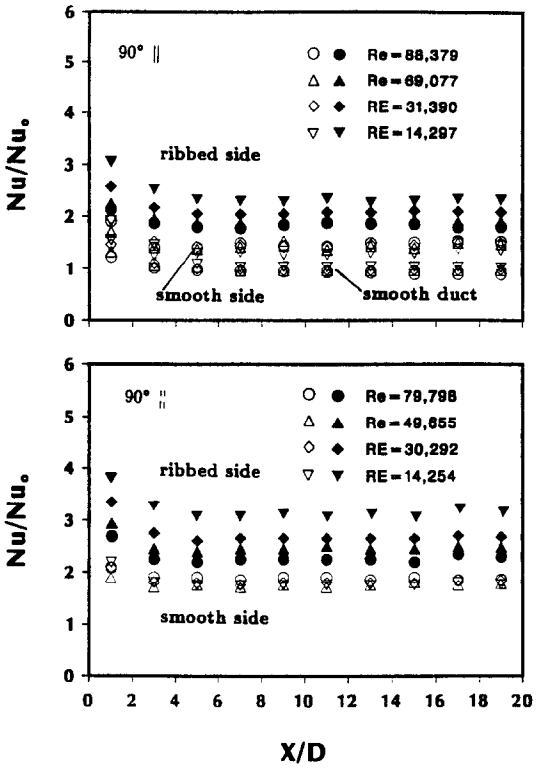

FIG. 3. Local Nusselt number ratio distributions for smooth channel and 90° rib.

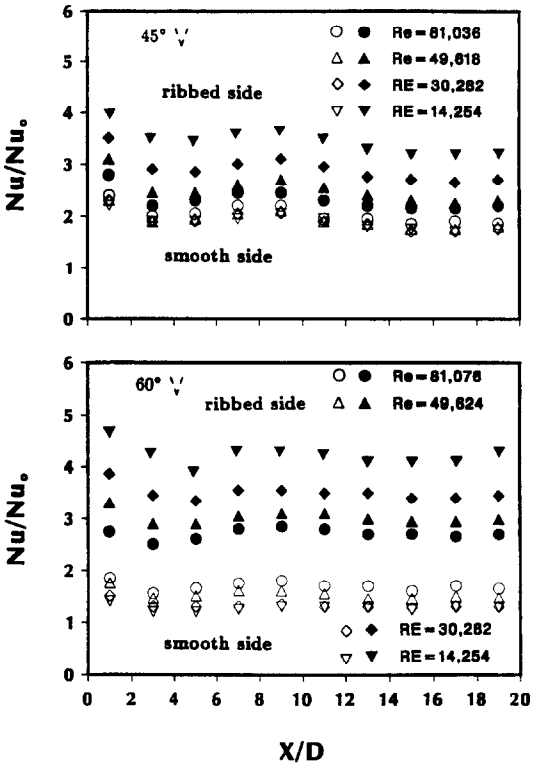

FIG. 5. Local Nusselt number ratio distributions for 45°/60° V-shaped broken ribs.

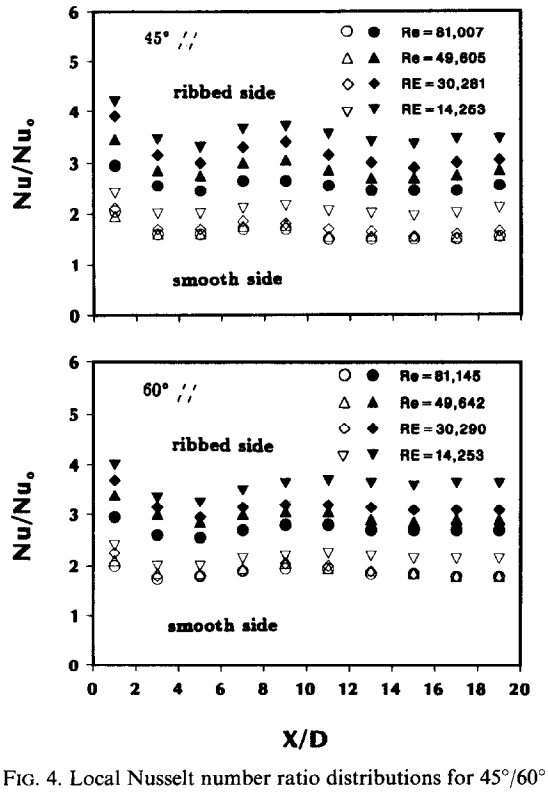

FIG. 4. Local Nusselt number ratio distributions for 45°/60° parallel broken rib.

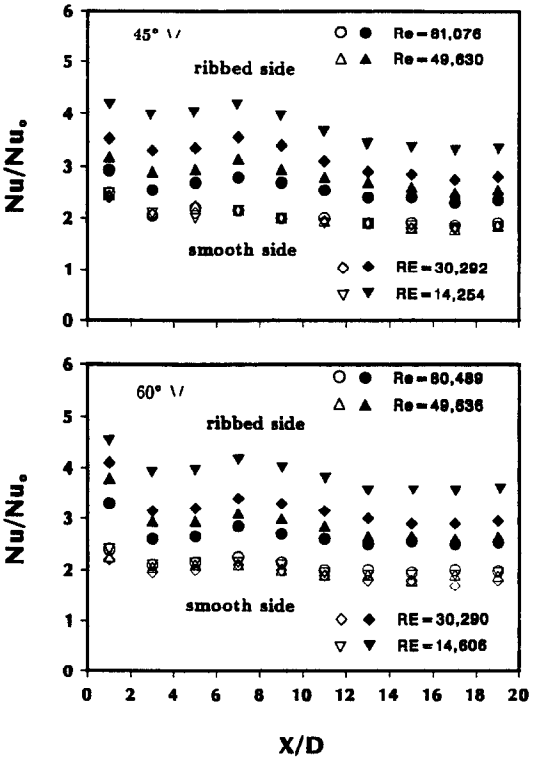

FIG. 6. Local Nusselt number ratio distributions for 45°/60° V-shaped broken ribs A.

number is the average value of the two opposite smooth-wall Nusselt numbers at a given location. The results show that for each case the local Nusselt number ratio decreases with increasing Reynolds number. For the cases of 90° continuous rib and 90° broken rib (Fig. 3), the Nusselt number ratio (ribbed-side or smooth-side) decreases while increasing the axial distance, and reaches a constant value in the fully developed region at a given flow Reynolds number. However, for the cases of 60° parallel broken rib and 45° parallel broken rib (Fig. 4), 60° V-shaped broken rib and 45° V-shaped broken rib (Fig. 5), and 60° V-shaped broken rib A and 45° V-shaped broken rib A (Fig. 6), the Nusselt number ratio (ribbed-side or smooth-side) decreases to reach a minimum value at X/D of around 4 and then increases to reach a maximum value at X/D of around 8 or 9. After the maximum value the Nusselt number ratio decreases slightly or maintains a constant value in the region further downstream.

The higher heat transfer coefficients obtained with broken V-shaped or broken parallel ribs are similar to those reported with continuous V-shaped or continuous parallel ribs in the previous studies [11]. It is conjectured that the flow pattern generated by the 60°/45° continuous parallel ribs contains two counter-rotating cells of secondary flow in the opposite near wall region of the square channel, while the 60°/45° continuous V-shaped ribs may generate two pairs of two counter-rotating cells along each divergent axis of V-shaped ribs (i.e. four counter-rotating cells of secondary flow) and cause a higher heat transfer [11]. Similarly, it is anticipated in this study that the 60°/45° broken V-shaped or broken parallel ribs may induce more counter-rotating cells of secondary flow and produce more local wall turbulence and cause an even higher heat transfer. The conjectured secondary flow induced by the broken ribs needs to be verified through the flow visualization technique and by the velocity profile measurements in a separate project.

Channel averaged heat transfer and pressure drop

Figure 7 shows the Nusselt number ratio (ribbed side or smooth side) vs Reynolds number for 90° continuous and 90° broken ribs, 60° and 45° V-shaped broken ribs, and 60° and 45° parallel broken ribs. The ribbed-side Nusselt number ratio is the average value of the entire ribbed-wall Nusselt number from the channel inlet to the outlet. Similarly, the smooth-side Nusselt number ratio is the average value of the entire smooth-wall Nusselt number from the inlet to the outlet of the heated channel. The results show that the 60° V-shaped broken rib provides higher Nusselt number ratios than the 60° parallel broken rib, and subsequently higher than other broken rib configurations. The 90° broken rib produces higher heat transfer than the 90° continuous rib but lower than any other broken rib studied. The 60° V-shaped broken rib gives the highest heat transfer in the ribbed-side wall but the lowest in the corresponding smooth-side wall. Figure 7 also shows that the Nusselt number ratio in the ribbed-side wall decreases with increasing Reynolds number, but the Nusselt number ratio in the smooth-side wall is insensitive to the Reynolds number. The rib orientation has a very significant influence on the ribbed-side wall Nusselt number ratio at lower Reynolds numbers, but the effect reduces at higher Reynolds numbers.

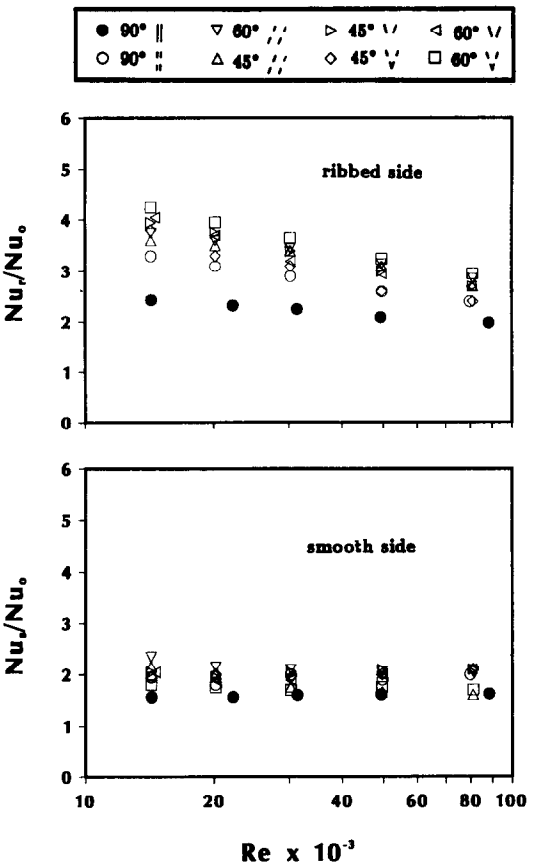

FIG. 7. Average Nusselt number ratio vs Reynolds number for studied broken rib configurations.

Figure 8 compares the friction factor ratio for eight rib configurations. The pressure drops across the test duct are measured at the unheated flow conditions. The results show that the 90° broken rib (and the 60° V-shaped broken rib A) and the 90° continuous rib (as well as the 45° parallel broken rib) provide the highest and lowest friction factor ratios, respectively. Also, the pressure drops for the cases of 60° parallel broken or V-shaped broken ribs are higher than those of 45° parallel broken or V-shaped broken ribs. Figure 8 shows that the friction factor ratio is insensitive to the Reynolds number.

Heat transfer performance comparison

Figure 9 represents the Nusselt number ratio of ribbed-side and smooth-side vs the friction factor ratio for parallel broken and V-shaped broken ribs (seven rib orientations, white symbols) over a range of Reynolds numbers between 15 000 and 80 000. The

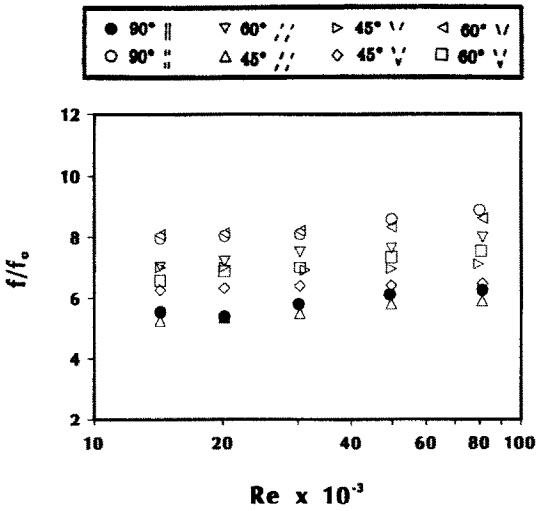

FIG. 8. Average friction factor ratio vs Reynolds number for studied broken rib configurations.

data for parallel continuous and V-shaped continuous ribs (five rib orientations, black symbols) from ref. [11] are included for direct comparison. The results show that, in general, the Nusselt number ratio increases with increasing friction factor ratio. The ribbed-side Nusselt number ratios for 60° and 45° parallel 'broken ribs' or V-shaped broken ribs are much higher than the corresponding 60° and 45° parallel 'continuous ribs' or V-shaped 'continuous ribs'. The 60° and 45° parallel 'broken ribs' or V-shaped broken ribs represent the similar characteristics of heat transfer augmentation and pressure drop increment in which the 60° V-shaped broken rib is the best. On the other hand, the 60° and 45° parallel 'continuous ribs' or V-shaped continuous ribs and the 90° broken and 90° continuous ribs have the same heat transfer and pressure drop characteristics in which the 60° V-shaped continuous ribs is the highest. In the broken rib group, the Nu_r/Nu_0 decreases with increasing Reynolds number but the f/f_0 is insensitive to the Reynolds number. In the continuous rib group, the Nu_r/Nu_0 decreases with increasing Reynolds number but the f/f_0 increases with increasing Reynolds number. The 60° V-shaped broken rib provides 3–4.2 times ribbed-side heat transfer augmentation with 7–8 times pressure drop penalty, while the 60° V-shaped continuous rib gives 2.7–3.5 times ribbed-side heat transfer enhancement with 8–11 times pressure drop penalty. In general, it is clear that the heat transfer enhancement is about 2.5–4 times for the broken rib group and 2–3 times for the continuous rib group for the same amount of pressure drop penalty. Note that the smooth-side heat transfer enhancement for the broken rib group is slightly lower than the continuous rib group.

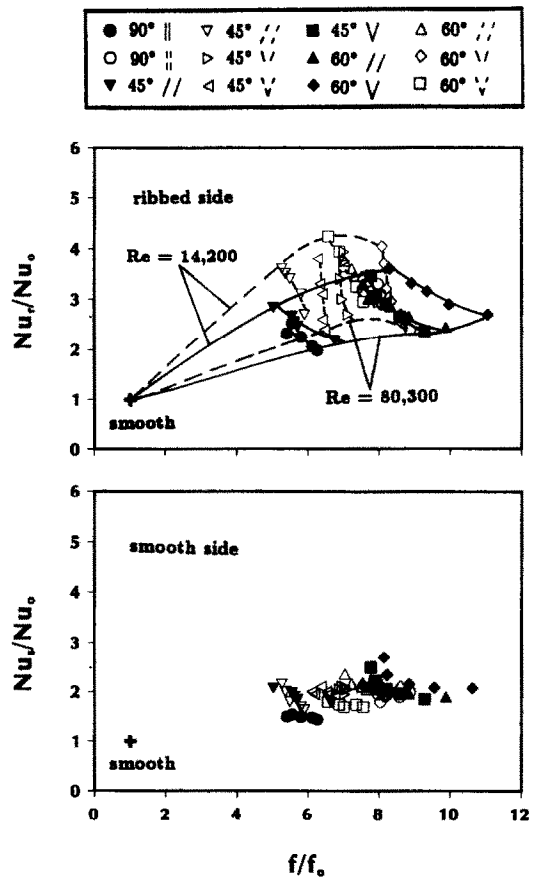

FIG. 9. Average Nusselt number ratio vs average friction factor ratio for broken ribs and comparison with previous continuous ribs.

Heat transfer and friction correlations

Figure 10 shows the friction roughness function (R) vs the roughness Reynolds number (e^+) for 90°, 60° and 45° broken ribs for a range of studied Reynolds numbers. The roughness function for the present 90° continuous ribs agrees with the previous correlation

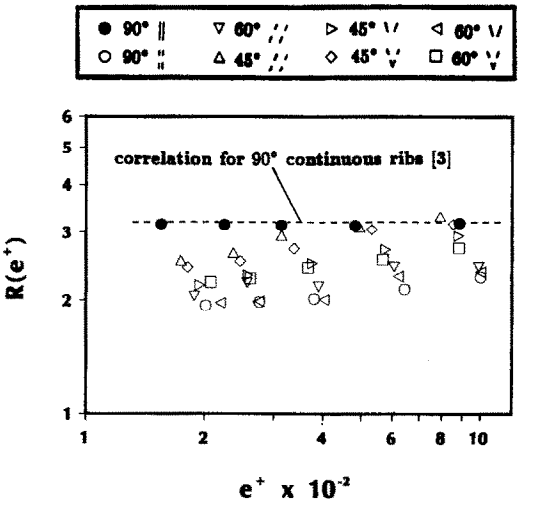

FIG. 10. Friction factor correlation.

Table 2. Coefficients and exponents for functions $R(e^+)$, $G(e^+)$ and $\bar{G}(e^+)$: $R(e^+) = a(e^+)^b$, $G(e^+) = a(e^+)^b$, $\bar{G}(e^+) = a(e^+)^b$

Case	a	b	a	b	a	b
90° ||	3.18	0.0	2.66	0.347	5.38	0.26
90° ⁞⁞	1.099	0.105	1.326	0.423	3.392	0.302
60° //	1.205	0.105	1.123	0.413	2.617	0.319
45° //	0.970	0.187	1.396	0.376	2.354	0.335
60° \/	1.049	0.145	1.041	0.424	2.542	0.329
45° \/	0.926	0.185	1.281	0.411	3.276	0.286
60° \/	0.923	0.137	1.348	0.405	3.647	0.278
45° \/	0.788	0.194	1.282	0.399	3.319	0.281

that was developed for the 90° continuous rib [3]. The 90° broken rib has the lowest roughness function, which implies the highest pressure drop. The roughness function (R) is almost independent of the roughness Reynolds number (e^+) for 90° continuous ribs studied. However, the roughness function increases with increasing roughness Reynolds number for all broken rib configurations studied. Table 2 gives the coefficients and exponents in this function for all cases studied. For a given rib configuration and flow Reynolds number, the friction factor can be predicted from the roughness function (R) read from Table 2. Note that the friction roughness function (R) shown in Fig. 10 is a universal result for each rib geometry independent of the e/D ratio. This has been verified for $0.021 \leqslant e/D \leqslant 0.063$ [1].

Figure 11 shows the heat transfer roughness function (G) vs the roughness Reynolds number (e^+) for 90°, 60° and 45° broken ribs for a range of Reynolds numbers studied. The similar types of drawings for the average heat transfer roughness function ($\bar{G}$), based on the average value of the ribbed-side and smooth-side heat transfer coefficients ($\overline{St}$), are also shown in Fig. 11. The heat transfer roughness function (G or $\bar{G}$) increases with the increase of the roughness Reynolds number (e^+) for all studied rib configurations. The heat transfer roughness function for 90° ribs is about the same as the previous correlation that was developed for the 90° continuous rib [3]. The 60° and 45° parallel broken ribs or 60° V-shaped broken rib have the lower G values, which means the higher heat transfer. Table 2 gives the coefficients and exponents in this function for all cases studied. The slopes of G vs e^+ for broken ribs are higher than that for the 90° transverse rib. However, the slopes of $\bar{G}$ vs e^+ for broken ribs are about the same as the 90° transverse rib. For a given rib configuration and flow Reynolds number, the Stanton number can be predicted from the heat transfer roughness function (G or $\bar{G}$) and roughness function (R) read from Table 2.

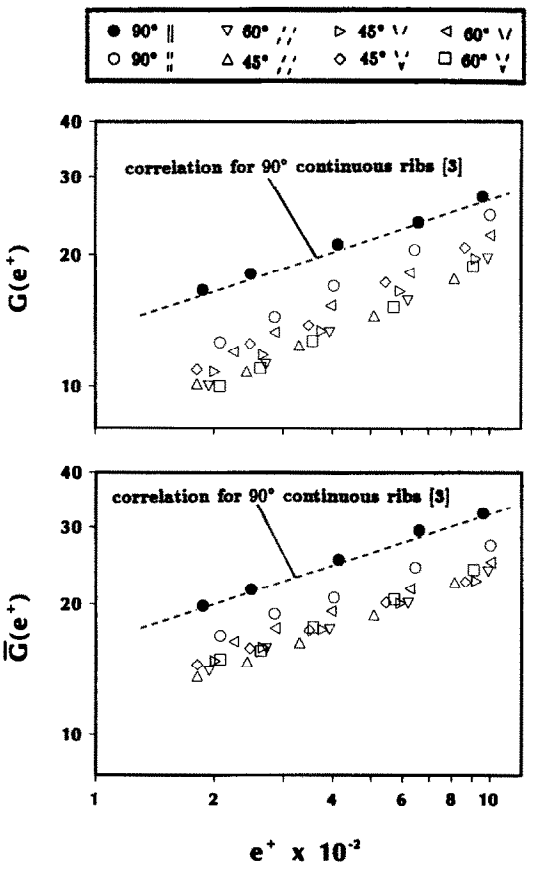

FIG. 11. Heat transfer correlation.

CONCLUDING REMARKS

Local heat transfer and pressure drop measurements have been performed in straight square channels with parallel broken and V-shaped broken ribs for Reynolds numbers from 15000 to 90000. The main findings of the study are given below.

(1) For 90° continuous or broken ribs, the Nusselt number ratio decreases by increasing the axial distance, and reaches a constant value several ribs from the channel entrance. For 60° or 45° parallel broken and 60° or 45° V-shaped broken ribs; however, the Nusselt number ratio decreases to a minimum and then increases to a maximum value downstream due to favorable secondary flow induced by rib orientation.

(2) For a range of studied Reynolds numbers, the 60° V-shaped broken rib gives higher heat transfer augmentation than other broken rib configurations while the 90° broken rib produces the largest pressure drop.

(3) The 60° parallel broken or 60° V-shaped broken ribs provide higher heat transfer augmentation than the 45° parallel broken or 45° V-shaped broken ribs. For all broken rib configurations, the heat transfer augmentation decreases with Reynolds numbers while the pressure drop increment is insensitive to Reynolds numbers.

(4) The 60° V-shaped 'broken ribs' or 60° parallel broken ribs perform better than the 60° V-shaped 'continuous ribs' or 60° parallel continuous ribs. The

heat transfer augmentation is about 2.5–4 times for the broken rib configurations and about 2–3 times for the continuous rib configurations with about 7–8 times pressure drop penalty.

(5) The semi-empirical correlations of the friction factor and Stanton number are developed for studied broken rib configurations that can be used for turbine cooling design.

Acknowledgments—The work was supported in part by the NSF (CBT-8713833) and the Texas Energy Research in Applications Program (TEES 32132-70730).

REFERENCES

1. J. C. Han, Heat transfer and friction in channels with two opposite rib-roughened walls, *ASME J. Heat Transfer* **106,** 774–781 (1984).
2. J. C. Han, J. S. Park and C. K. Lei, Heat transfer enhancement in channels with turbulence promoters, *ASME J. Engng Gas Turbines Pwr* **107,** 629–635 (1985).
3. J. C. Han, Heat transfer and friction characteristics in rectangular channels with rib turbulators, *ASME J. Heat Transfer* **110,** 321–328 (1988).
4. J. C. Han and J. S. Park, Developing heat transfer in rectangular channels with rib turbulators, *Int. J. Heat Mass Transfer* **31,** 183–195 (1988).
5. J. C. Han, S. Ou, J. S. Park and C. K. Lei, Augmented heat transfer in rectangular channels of narrow aspect ratios with rib turbulators, *Int. J. Heat Mass Transfer* **32,** 1619–1630 (1989).
6. J. C. Han, P. R. Chandra and S. C. Lau, Local heat/mass transfer distributions around sharp 180° turns in two-pass smooth and rib-roughened channels, *ASME J. Heat Transfer* **110,** 91–98 (1988).
7. P. R. Chandra, J. C. Han and S. C. Lau, Effect of rib angle on local heat/mass transfer distribution in a two-pass rib roughened channel, *ASME J. Turbomachinery* **110,** 233–241 (1988).
8. P. R. Chandra and J. C. Han, Pressure drop and mass transfer in two-pass ribbed channels, *AIAA J. Thermophys. Heat Transfer* **3,** 315–320 (1989).
9. J. C. Han and P. Zhang, Pressure loss distribution in three-pass rectangular channels with rib turbulators, *ASME J. Turbomachinery* **111,** 515–521 (1989).
10. J. C. Han and P. Zhang, Effect of rib-angle orientation on local mass transfer distribution in a three-pass rib-roughened channel, *ASME J. Turbomachinery* **113,** 123–130 (1991).
11. J. C. Han, Y. M. Zhang and C. P. Lee, Augmented heat transfer in square channels with parallel, crossed, and V-shaped angled ribs, *ASME J. Heat Transfer* **113,** 590–596 (1991).
12. F. Burggraf, Experimental heat transfer and pressure drop with two-dimensional turbulence promoter applied to two opposite walls of a square tube. In *Augmentation of Convective Heat and Mass Transfer* (Edited by A. E. Bergles and R. L. Webb), pp. 70–79. ASME, New York (1970).
13. D. E. Metzger and M. K. Sahm, Heat transfer around sharp 180° turns in smooth rectangular channels, *ASME J. Heat Transfer* **108,** 500–506 (1986).
14. R. L. Webb, E. R. G. Eckert and R. J. Goldstein, Heat transfer and friction in tubes with repeated-rib roughness, *Int. J. Heat Mass Transfer* **14,** 601–617 (1971).
15. D. L. Gee and R. L. Webb, Forced convection heat transfer in helically rib-roughened tubes, *Int. J. Heat Mass Transfer* **23,** 1127–1136 (1980).
16. R. Sethumadhavan and M. Raja Rao, Turbulent flow heat transfer and fluid friction in helical-wire-coil-inserted tubes, *Int. J. Heat Mass Transfer* **26,** 1833–1844 (1983).
17. J. C. Han, L. R. Glicksman and W. M. Rohsenow, An investigation of heat transfer and friction for rib-roughened surfaces, *Int. J. Heat Mass Transfer* **21,** 1143–1156 (1978).
18. D. E. Metzger and R. P. Vedula, Heat transfer in triangular channels with angled roughness ribs on two walls, *Expl Heat Transfer* **1,** 31–44 (1987).
19. M. Dalle Donne and L. Meyer, Turbulent convective heat transfer from rough surfaces with two-dimensional rectangular ribs, *Int. J. Heat Mass Transfer* **20,** 582–620 (1977).
20. L. Meyer, Thermohydraulic characteristics of single rods with three-dimensional roughness, *Int. J. Heat Mass Transfer* **25,** 1043–1058 (1982).
21. S. J. Kline and F. A. McClintock, Describing uncertainties in single-sample experiments, *Mech. Engng* **75,** 3–8 (1953).
22. W. M. Rohsenow and H. Choi, *Heat, Mass and Momentum Transfer*, pp. 56–59, 192–193. Prentice-Hall, Englewood Cliffs, New Jersey (1961).

CANAUX A HAUTE PERFORMANCE DE TRANSFERT THERMIQUE AVEC NERVURES ROMPUES PARALLELES OU EN V

Résumé—On étudie l'effet de l'orientation de nervures brisées sur les distributions de transfert thermique et la perte de pression dans un canal carré avec deux parois opposées et nervurées en ligne, pour des nombres de Reynolds entre 15 000 et 90 000. Le conduit carré est composé de dix sections isolées en cuivre et il y a un rapport longueur sur diamètre hydraulique de 20. Le rapport hauteur sur diamètre hydraulique des nervures est 0,0625 et le pas rapporté à la hauteur de la nervure est égal à 10. Les résultats montrent que la nervure rompue à 60° parallèle ou à 60° en V fournit un accroissement de transfert thermique plus élevé que la nervure rompue à 45° parallèle ou à 45° en V et aussi plus grand que la nervure rompue à 90°. La nervure rompue parallèle ou en V conduit à une augmentation de transfert 2.5 à 4 fois supérieure au cas des nervures continues parallèles ou en V, avec une augmentation de 2 à 3 fois pour le même accroissement pénalisant de 7–8 fois la perte de pression.

HOCHLEISTUNGSWÄRMEÜBERGANGSKANÄLE MIT PARALLELEN ODER V-FÖRMIG UNTERBROCHENEN RIPPEN

Zusammenfassung—In der vorliegenden Arbeit werden die Auswirkungen der Ausrichtung von unterbrochenen Rippen auf die örtliche Verteilung des Wärmeübergangs und den Druckabfall in einem quadratischen Kanal mit zwei längsberippten, gegenüberliegenden Wänden für Reynolds-Zahlen von 15000 bis 90000 untersucht. Der quadratische Kanal besteht aus zehn isolierten Kupferteilen und hat ein Verhältnis von Länge zu hydraulischem Durchmesser von 20. Das Verhältnis von Rippenhöhe zu hydraulischem Durchmesser beträgt 0,0625, das Verhältnis von Rippenteilung zu Rippenhöhe beträgt 10. Die Ergebnisse zeigen, daß die um 60 Grad gedrehten parallelen oder V-förmigen unterbrochenen Rippen eine stärkere Verbesserung des Wärmeübergangs aufweisen als solche, die um 45 Grad oder um 90 Grad gedreht sind. Der Wärmeübergang erhöht sich bei den beschriebenen unterbrochenen Rippen um das 2.5- bis 4-fache gegenüber einer 2- bis 3-fachen Erhöhung bei den früheren parallelen oder V-förmigen kontinuierlichen Rippen. Der Druckabfall erhöht sich in beiden Fällen um das 7- bis 8-fache.

ВЫСОКОЭФФЕКТИВНЫЕ ТЕПЛООБМЕННЫЕ КАНАЛЫ С ПАРАЛЛЕЛЬНЫМИ ПРЕРЫВИСТЫМИ И ПРЕРЫВИСТЫМИ *V*-ОБРАЗНЫМИ РЕБРАМИ

Аннотация—Исследуется влияние прерывистой ориентации ребер на локальные распределения теплопереноса и перепад давления в канале квадратного сечения с коридорным оребрением на двух противоположных стенках при изменении чисел Рейнольдса от 15000 до 90000. Канал состоит из десяти изолированных медных секций и имеет отношение длины к гидравлическому диаметру, равное 20. Отношение высоты ребра к гидравлическому диаметру составляет 0,0625, а отношение шага ребер к их высоте равно 10. Полученные результаты показывают, что параллельные прерывистые ребра с углом 60° или *V*-образные прерывистые ребра с таким же углом обеспечивают более существенную интенсификацию теплопереноса, чем те же ребра с углом 45° и, следовательно, чем прерывистые ребра с углом 90°. В случае параллельных или *V*-образных "прерывистых ребер" теплоперенос возрастает в 2.5–4 раза по сравнению с ранее исследованными параллельными или *V*-образными сплошными ребрами, при которых теплообмен интенсифицируется в 2–3 раза при том же 7–8-кратном росте перепада давления.